

Chemical Science

Accepted Manuscript



This article can be cited before page numbers have been issued, to do this please use: Z. Wu, T. Wang, Y. Meng, Y. Rao, S. Gao, J. Zheng, B. Wang and J. Zhang, *Chem. Sci.*, 2017, DOI: 10.1039/C7SC02073B.



This is an Accepted Manuscript, which has been through the Royal Society of Chemistry peer review process and has been accepted for publication.

Accepted Manuscripts are published online shortly after acceptance, before technical editing, formatting and proof reading. Using this free service, authors can make their results available to the community, in citable form, before we publish the edited article. We will replace this Accepted Manuscript with the edited and formatted Advance Article as soon as it is available.

You can find more information about Accepted Manuscripts in the [author guidelines](#).

Please note that technical editing may introduce minor changes to the text and/or graphics, which may alter content. The journal's standard [Terms & Conditions](#) and the ethical guidelines, outlined in our [author and reviewer resource centre](#), still apply. In no event shall the Royal Society of Chemistry be held responsible for any errors or omissions in this Accepted Manuscript or any consequences arising from the use of any information it contains.



Journal Name

ARTICLE

Enhancing the Reactivity of Nickel(II) in Hydrogen Evolution Reactions (HER) by β -Hydrogenation of Porphyrinoid Ligands

Received 00th January 20xx,
Accepted 00th January 20xx

DOI: 10.1039/x0xx00000x

www.rsc.org/

Zhuo-Yan Wu^a, Teng Wang^a, Yin-Shan Meng^a, Yu Rao^a, Bing-Wu Wang^{a*}, Jie Zheng^{a*}, Song Gao^a and Jun-Long Zhang^{a*}

Fine-tuning of porphyrin β -periphery is important for naturally occurring metal tetrapyrroles to exert diverse biological roles. Here we described that this approach is also applied to design molecular catalysts, as exemplified by Ni(II) porphyrinoids catalyzing hydrogen evolution reaction (HER). We found that β -hydrogenation of porphyrin remarkably enhances electrocatalytic HER reactivity (turnover frequencies of 6287 vs. 265 s⁻¹ for Ni(II) chlorin Ni-2 and porphyrin Ni-1, and of 1737 vs. 342 s⁻¹ for Ni(II) hydroporpholactone Ni-4 and porpholactone Ni-3, respectively) using trifluoroacetic acid (TFA) as the proton source. DFT calculations suggest that, after two-electron reduction, β -hydrogenation renders more electron density located on the Ni center and thus prefers to generate highly reactive nickel hydride intermediate. To demonstrate it, decamethylcobaltocene Co(Cp*)₂ was used as a chemical reductant, [Ni-2]²⁻ reacts *ca.* 30 times faster than [Ni-1]²⁻ with TFA, in line with the electrocatalysis and computational results. Thus, such subtle structural changes inducing the distinctive reactivity of Ni(II) not only tests the fundamental understanding of natural Ni tetrapyrroles also provides a valuable clue to design metal porphyrinoid catalysts.

Introduction

Fine-tuning of porphyrin β -periphery is important for the naturally occurring metal tetrapyrroles to exert diverse biological functions within a broad structural similarity.^{1a, 1b, 1c, 1d, 1e} As a consequence of theoretical and modeling studies on the structural–electronic–functional relationship, β -hydrogenation of porphyrins attracts much attention for lowering the molecular symmetry and altering the energy level of frontier molecular orbitals by the subtle structural changes, especially in mimicking light harvesting antenna,^{2a, 2b} photosensitizers^{3a, 3b} and the related optoelectronic materials.^{4a, 4b, 4c} In contrast to tremendous progress in the physicochemical properties, applying the structural insights gained from natural tetrapyrroles to catalysis had been long ignored. In fact, β -modification is in equal importance for metalloenzymes, as exemplified by Ni(II) tetrapyrrole cofactors found in reductases.^{5a, 5b} These Ni cofactors such as F₄₃₀

coenzymes^{6a, 6b} and tunichlorin^{7a, 7b} possess either corphin or chlorin, featured at least one reduced pyrrole, other than protoporphyrin. The interrupted conjugation arising from the reduced pyrrole(s) renders the distortions of porphyrin ring, larger binding cavity and more electron rich Ni center after one or two electron reduction, as revealed by electrochemical studies on β -hydroporphyrin models.^{8a, 8b, 8c, 8d} Encouraged by these pioneer studies, we herein reported the first example that β -hydrogenation of porphyrinoids significantly enhances the reactivity of nickel(II) in hydrogen evolution reaction (HER), which demonstrates the importance of bioinspired β -modification on designing molecular catalysts.

Hydrogen evolution reaction (HER) is a fundamental process in water splitting to produce hydrogen energy potentially

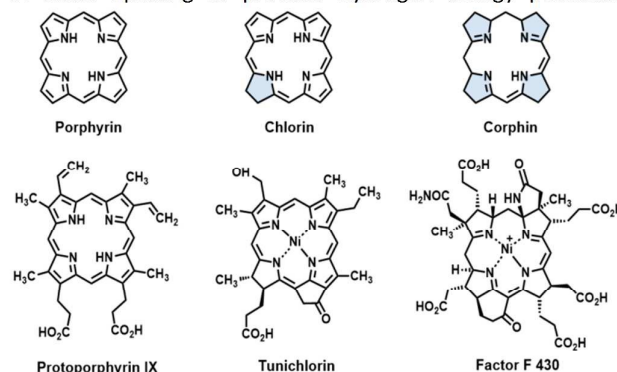


Fig. 1 Selected examples for natural tetrapyrroles and synthetic models.

^a Z.-Y. Wu, T. Wang, Y.-S. Meng, Y. Rao, Profs. S. Gao, B.-W. Wang, J. Zheng and J.-L. Zhang

Beijing National Laboratory for Molecular Sciences
State Key Laboratory of Rare Earth Materials Chemistry and Applications, College of Chemistry and Molecular Engineering
Peking University
Beijing 100871 (P.R. China)

E-mail: zhangjunlong@pku.edu.cn, wangbw@pku.edu.cn, zhengjie@pku.edu.cn.

^b Supporting information for this article is given via a link at the end of the document.



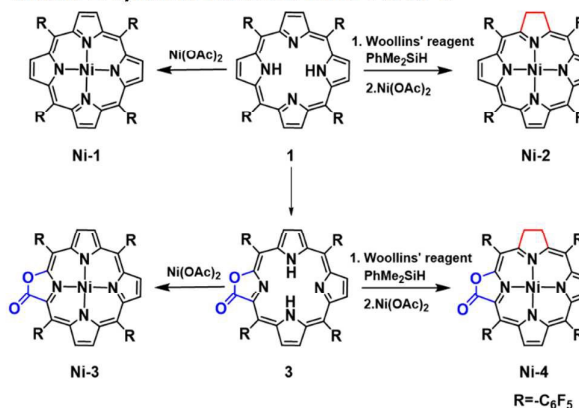
ARTICLE

Journal Name

alternative to traditional fossil fuels.^{9a, 9b, 9c, 9d} On the road of seeking earth-abundant metals to replace noble metals,^{10a, 10b, 10c, 10d, 10e, 10f} nickel(II) complexes of porphyrins have attracted increasing attentions for the combination of the pivotal role of Ni(II) in [NiFe] hydrogenases^{11a, 11b} and the sophisticate porphyrin chemistry.^{12a, 12b, 12c, 12d, 12e} Recently Cao and co-workers proposed a one-electron reduction and bimetallic homolysis mechanism based on Ni(II) porphyrin with *meso*-pentafluorophenyl substituents.¹³ Nocera and co-workers constructed a “2nd coordination sphere” around Ni(II) center using a hangman type porphyrin, which demonstrated hydrogen bond facilitating proton coupled electron transfer process.¹⁴ More importantly, the same group found a Ni(II) phlorin intermediate during HER, in which a proton was added to *meso*-carbon appended to the hangman moiety.¹⁵ The appearance of phlorin intermediate implies the necessary to investigate the hydroporphyrin with interrupted conjugation.

As our continued effort to unravel the roles of β -modification on the functions of porphyrins,^{16a, 16b, 16c, 16d} in the present study, we reported the synthesis, electrochemical characterization and HER reactivity of nickel complexes of porphyrin (Ni-1), chlorin (Ni-2), porpholactone (Ni-3) and β -hydroporpholactone (Ni-4). Importantly, as a results of β -hydrogenation, Ni-2 and Ni-4 exhibited significantly enhanced electrocatalytic HER reactivity (determined by turnover frequencies, TOFs) of 24 and 5 times than the corresponding porphyrin (Ni-1) and porpholactone (Ni-3) respectively. More importantly, DFT calculation suggests that, β -hydrogenation renders more electron rich Ni centers in two-electron reduced [Ni-2]²⁻ and [Ni-4]²⁻ than the analogues [Ni-1]²⁻ and [Ni-3]²⁻, and

Scheme 1. Synthetic Procedure for Ni-1 to Ni-4.



thus tend to form active nickel hydride intermediates. This is supported by the titration of trifluoroacetic acid (TFA) to two-electron reduced nickel complexes, in which [Ni-2]²⁻ reacts *ca.* 30 times faster than [Ni-1]²⁻. Therefore, this work demonstrated that such a subtle structural modification inspired by nature is instrumental to the observation and investigation of catalytic properties of metal porphyrinoid complexes.

Results and discussion

Synthesis and Characterization. In this work, free-base porphyrinoids 1-4 were synthesized in good yields according to the literatures.^{16c, 17} Nickel complexes (Scheme 1.) were prepared by refluxing excess nickel(II) acetate (30 *equiv.*) with

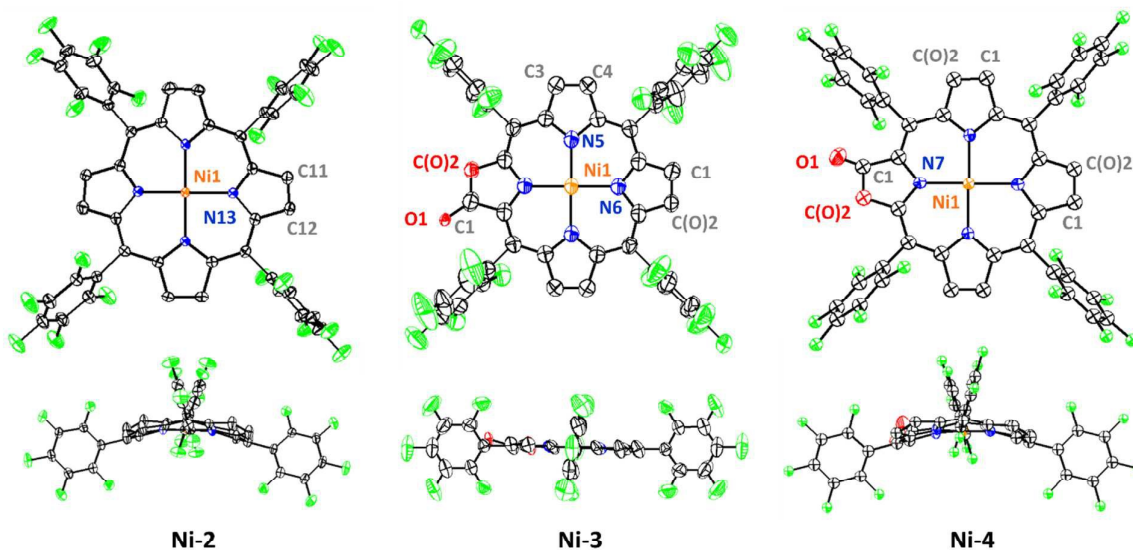


Fig. 2 ORTEP drawings of Ni-2, Ni-3 and Ni-4. The hydrogen atoms and solvent molecules are omitted for clarity. Thermal ellipsoids are drawn with 50% probability. The lactone ring in Ni-3 shows disorder at the oxazolone and the opposite position while the Ni-4 and Ni-2 show disorder at all four β -periphery.



the corresponding porphyrinoid ligands in dimethylformamide (DMF) under N_2 atmosphere. Four nickel complexes were fully characterized by UV-vis absorption, 1H , ^{19}F , ^{13}C -NMR and HR ESI-MS spectroscopies and spectrometers (Supporting information). Ni-2 and Ni-4 were diamagnetic for the low spin d^8 electronic structure and showed the proton signals at 3.93 and 3.77-3.65 ppm, respectively, assigned to the hydropyrrole moiety. Compared to Ni-1 and Ni-3, β -hydro-analogues Ni-2 and Ni-4 exhibited two bathochromic Q-bands centered at 576 or 565 and 617 or 613 nm in acetonitrile, which is also the characteristic absorption of metal chlorins arising from the lower molecular symmetry.

Crystal of Ni-2, Ni-3 and Ni-4 were obtained by slow evaporation of a dichloroethane/*n*-hexane solution. As shown in Fig. 2, the crystal structure of Ni-2 (CCDC: 1528290) displayed the typical ruffling distortion with Ni atom centered at N4 planar squares. Although it is difficult to distinguish the hydropyrrole ring from the other ones due to the symmetry condition of the $I\bar{4}2d$ space group, the average pyrrole C-C bond length (C2-C3, 1.383 Å) of Ni-2 is 0.04 Å longer than that of Ni-1 (C11-C13, 1.346 Å)¹³. Similarly, the hydropyrrole ring on Ni-3 (CCDC: 1554494) can be distinguished through comparison of the C-C bond length with Ni-4 (CCDC:1554445) (C1-C(O)2, 1.338 Å and C3-C4, 1.341 Å for Ni-3 and C1-C(O)2, 1.404 Å for Ni-4). In addition, Ni-4 display a typical ruffling distortion with Ni-N bond of 1.921 Å, however, Ni-3 displays a planar construction with Ni-N bond of 1.950 Å. The shorter Ni-N bond induces steric strain to Ni-4, the release of which is the driving force for easier reduction of the nickel complexes.^{1b}

Electrochemistry. Cyclic voltammograms of Ni complexes in acetonitrile using 0.10 M nBu_4NPF_6 as supporting electrolyte

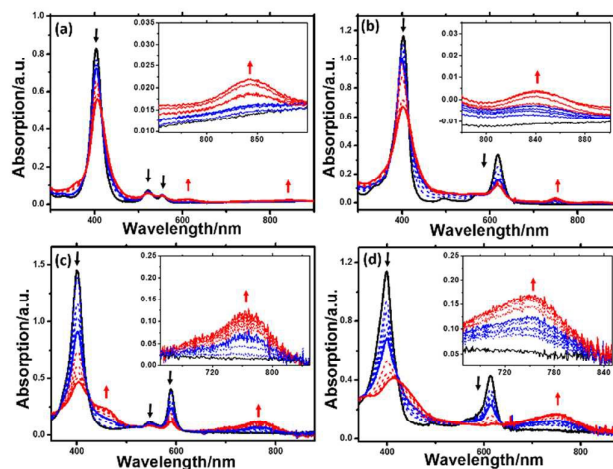


Fig. 3 UV-vis absorption spectra of (a): Ni-1 (Black), [Ni-1] $^{\bullet}$ (blue), and [Ni-1] $^{2\bullet+}$ (red), (b): Ni-2 (Black), [Ni-2] $^{\bullet}$ (blue), and [Ni-2] $^{2\bullet+}$ (red) (c): Ni-3 (Black), [Ni-3] $^{\bullet}$ (blue), and [Ni-3] $^{2\bullet+}$ (red), (d): Ni-4 (Black), [Ni-4] $^{\bullet}$ (blue), and [Ni-4] $^{2\bullet+}$ (red) in acetonitrile using the thin-layer spectroelectrochemistry. Insets: Enlarged view of absorbance of 750–850nm for Ni-1 and Ni-2, 700–840 nm for Ni-3 and Ni-4.

were shown in Fig. S18. Both Ni-1 and Ni-2 displayed two distinct reversible one-electron diffusion controlled reductions (-1.27 and -1.83 V for Ni-1, -1.28 and -1.77 V for Ni-2), referenced to the standard reduction potential of Fc^+/Fc . According to the previous reports,^{18a, 18b} the insertion of electron deficient oxazolone moiety lowers the energy levels of ligand LUMOs and thus we could observe the positive shift of reduction potentials of Ni-3 to Ni-1. However, Ni-4 displayed more negative reduction potentials than Ni-3 (-0.99 and -1.59 V for Ni-3, -1.14 and -1.74 V for Ni-4), indicating β -hydrogenation increases the energy levels of LUMOs in porpholactones.

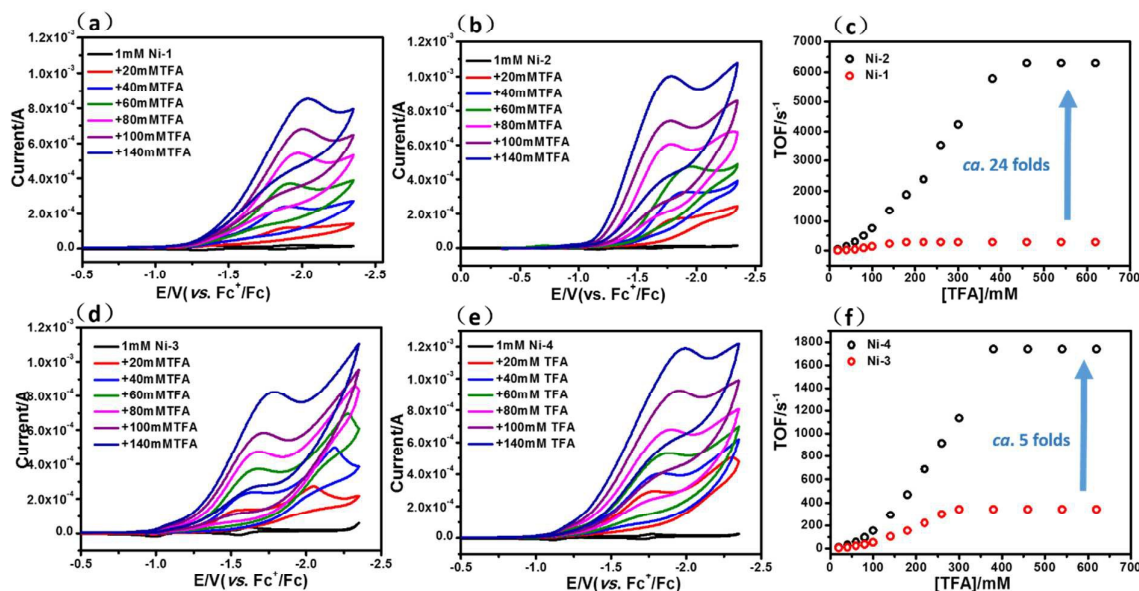


Fig. 4 Successive cyclic voltammograms of 1.0 mM Ni-1 (a) Ni-2 (b) Ni-3 (d) and Ni-4 (e) in CH_3CN (0.10 M nBu_4NPF_6) at increasing concentrations of TFA from 20 mM to 140 mM. Conditions: 3 mm glassy-carbon working electrode; 25 $^{\circ}C$; scan rate 100 mV/s. (c) and (f) TOFs vs. concentrations of TFA.

1
2
3

4

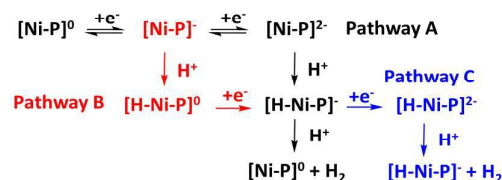


Spectroelectrochemistry of Ni(II) complexes was performed to monitor the spectral changes during the reduction process. As shown in Fig. 3, one-electron reduction (*ca.* -1.3 V) of Ni-1 and Ni-2 caused a slight decrease and hypsochromic shift on the Soret and Q bands, suggesting the formation of formally Ni^{II/I} couple according to previous studies by Savéant¹⁹ and Brückner²⁰ and others^{21a, 21b}. When *ca.* -1.85 V was applied, the Soret band and Q bands of [Ni-1]²⁻ decreased in intensity, accompanied with two broad bands appeared at 621 and 850 nm, and thus indicated the formation of a typical porphyrinic dianion.^{8a, 22} For [Ni-2]²⁻, an appearance of a broad band centered at 752 nm is assigned to porphyrin π -anion radical.^{8a, 23a, 23b} This assignment is also supported by DFT calculation results in the context. For porpholactone analogues Ni-3 and Ni-4, it is difficult to distinguish the electronic structures from the UV-vis spectra. When they were reduced at *ca.* -1.2 or -1.85 V, the intensity of Soret and Q bands decreased with red-shift and the absorption centered at 750 nm appeared, indicating the electrons delocalized on the macrocycle. Definitive assignment of the electronic structures of Ni complexes will be further discussed by DFT calculation in the context.

Electrocatalysis Hydrogen Production. HER activities of the four nickel(II) complexes were evaluated by successive cyclic voltammograms in acetonitrile using TFA ($pK_a = 12.7$ in CH₃CN) as a proton source. Electrocatalytic production of H₂ was confirmed by gas chromatographic analysis, and the Faradaic yields for the four complexes were obtained almost above 90% based on the amount of H₂ produced (Fig. S21). There is no observable decomposition of Ni complexes during HER, according to LDS (Fig. S22), TEM (Fig. S23) and UV-vis absorption spectra (Fig. S26) of the reaction solution before and after the electrolysis. In addition, SEM and EDX (Fig. S25) of the glassy carbon working electrode before and after the HER reaction showed no nickel films deposited on the electrode and thus excludes the possibility of free Ni(II) ion from Ni complexes as active species. The HER experiments using the dissolved Ni(II) salts of Ni(OTf)₂ (Fig. S24) shows relatively high overpotential and low catalytic activity, thus we excluded the possibility of the dissolved Ni(II) salts as active intermediates.

In presence of TFA, an S-shaped irreversible catalytic response for proton reduction triggered at *ca.* -1.80 V can be observed for four nickel complexes, as shown in Fig. 4. As shown in Fig. 4c and S19, Ni-1 reached its maximum turnover frequencies when applied with 180 mM TFA (Fig. S19). Here, we roughly estimated the maximum TOF of 265 s⁻¹ from eq. 1

Scheme 2. Possible heterolytic reaction pathways in nickel porphyrin catalyzed HER process



in supporting information for Ni-1 from the ratio of the maximum catalytic current i_{cat} to the peak current i_p (i_{cat}/i_p) with TFA (180 mM). Surprisingly, Ni-2 displayed significantly enhanced catalytic reactivity up to the maximum TOF of 6287 s⁻¹ (*ca.* 24 times than Ni-1) when the concentration of TFA reaches 460 mM. Similar enhancement of HER reactivity (Fig. S19) but to a lesser extent was observed by comparison of Ni-3 and Ni-4, in which the later exhibited almost 5 times TOF (1737 s⁻¹) than Ni-3 (342 s⁻¹). The value of TOF have also been confirmed by FOWA method (Fig. S27)^{24a, 24b}, the results from the two methods show the same trend that the β -hydrogenation of the pyrrole ring enhance the reactivities of nickel porphyrinoids with the TOF of Ni-2 > Ni-1, and Ni-4 > Ni-3. And It is worthy to note that the replacement of β -lactone moiety results comparable reactivity to the porphyrin analogue (Ni-1 vs. Ni-3) but much lower reactivity than chlorin complex (Ni-2 vs. Ni-4). Thus, these results clearly demonstrated that β -hydrogenation of porphyrin or porpholactone can remarkably enhance catalytic HER reactivity.

With the plateau current of the catalytic S-shaped voltammograms appearing at the second reduction peak of the nickel complexes, we considered that electrochemical-electrochemical-chemical-chemical (EECC) mechanism (pathway A) might be the most possible mechanism.²⁵ However other reaction pathways cannot be excluded. The catalytic onset can appear at the first reduction

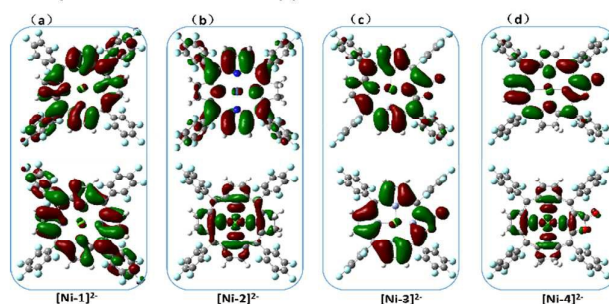


Fig. 5 Calculated (B3LYP) SOMO+1 (up) and SOMO (below) of [Ni-1]²⁻ (a), [Ni-2]²⁻ (b), [Ni-3]²⁻ (c) and [Ni-4]²⁻ (d) showing the different electronic structures.





Journal Name

ARTICLE

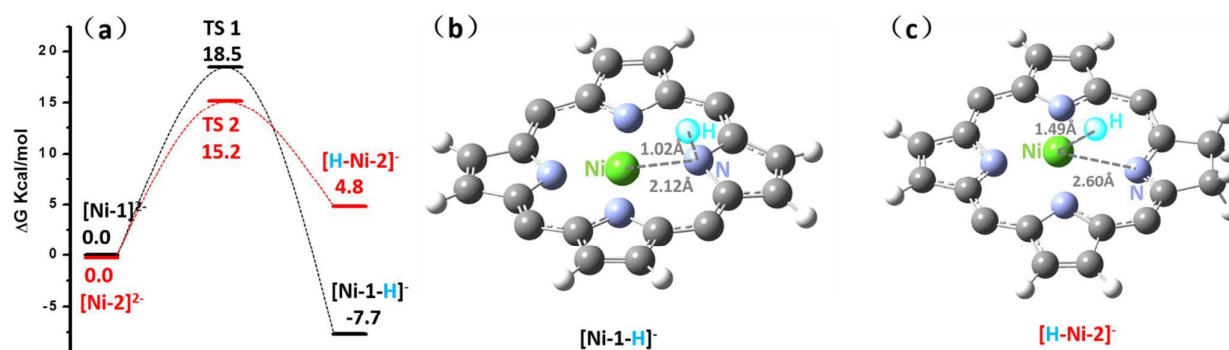


Fig. 6 (a) Free energy diagram for the formation of $[\text{Ni-1-H}]^-$ (black line) and $[\text{H-Ni-2}]^-$ (red line) intermediates during the HER process. Free-energy values are given in kcal/mol. The geometric conformation of $[\text{Ni-1-H}]^-$ (b) and $[\text{H-Ni-2}]^-$ (c) active intermediates during the HER process.

wave with stronger acid such as methylsulfonic acid (MsOH) (Fig. S28). In this situation, the acid might be strong enough to hydrogenate $[\text{Ni-P}]$ to $[\text{H-Ni-P}]^0$ which then be reduced to $[\text{H-Ni-P}]^-$ and react with another proton to yield hydrogen (pathway B). This phenomenon has been reported by Nocera¹⁵ and Cao¹³ respectively. In addition, at low acid concentration, we can observe another catalytic plateau after the catalytic current raised up at the second reduction peak in Ni-3. In this situation, the $[\text{H-Ni-P}]^-$ might be further reduced to $[\text{H-Ni-P}]^{2-}$ and then react with a proton to release H_2 and be back to $[\text{Ni-P}]^-$ (pathway C), as Savéant and co-workers previously reported.²⁶

Electronic Structures of Ni-1 to Ni-4. To understand the effect of β -hydrogenation on porphyrins on the reactivity of Ni complexes, DFT calculations were carried out to optimize the electronic structures (See more computation details in supporting information). The most stable form of $[\text{Ni-1}]^0$, $[\text{Ni-2}]^0$ and $[\text{Ni-4}]^0$ are all saddle-shaped closed-shell singlet, and $[\text{Ni-3}]^0$ is in flat closed-shell singlet, in accordance with the $^1\text{H-NMR}$ spectra and crystal structures. One-electron reduced nickel complexes have the most stable doublet flat geometries with an Mulliken spin density (ρ_{Ni}) of approximate 1.0 on Ni center, indicating a formally Ni(I) specie. Interestingly, two-electron reduced nickel complexes have different electronic structures as shown in Fig. 5. For $[\text{Ni-1}]^{2-}$ and $[\text{Ni-3}]^{2-}$, the flat triplet is lower in energy than the closed-shell bent singlet and two unpaired electron localized on the porphyrin macrocycle. Small Mulliken spin density ρ_{Ni} s of 0.0026 and 0.36 were obtained for $[\text{Ni-1}]^{2-}$ and $[\text{Ni-3}]^{2-}$ respectively (Table S9 and S11), suggesting a Ni(II) porphyrin diradical consistent to the

above spectroelectrochemistry results. Additionally, singly occupied molecular orbital (SOMO) of $[\text{Ni-1}]^{2-}$ and $[\text{Ni-3}]^{2-}$ also showed the electron density almost located on porphyrin β -periphery (Fig. 5a and 5c). However, Nocera and his coworker's report an analogue of $[\text{Ni-1}]^{2-}$ (*meso*-chlorine atoms were used to replace *meso*-pentafluorophenyl substituents of nickel porphyrin in his work) is a flat triplet species with a Mulliken spin density of almost 1 on the Ni center and almost 1 on the ligands.¹⁵ As shown in Fig. S34, we find that *meso*-substitutional group would affect the calculation results. In addition, five different DFT functionals have been used (B3LYP, B3P86, BP86, BLYP and M06L) to confirm our results. This indicated that using 6-31+G(d) as basis set and LAN2DZ as pseudopotential and B3LYP as functional is reasonable.

In sharp contrast, two-electron reduced $[\text{Ni-2}]^{2-}$ and $[\text{Ni-4}]^{2-}$ possess the most stable flat triplet with the Mulliken spin density on nickel center of $\rho_{\text{Ni}} = 1.22$ and 0.95 (Table S10 and S12), indicating that one unpaired electron is localized on nickel center and another on the macrocycle. Calculated SOMOs of $[\text{Ni-2}]^{2-}$ and $[\text{Ni-4}]^{2-}$ also showed that one unpaired electron is localized on the $\sigma^*(d_{x^2-y^2})$ orbital of Ni center, and another delocalized on the porphyrin, indicating a Ni(II) porphyrin radical (Fig. 5b and 5d).

DFT Calculated formations of $[\text{Ni-1-H}]^-$ and $[\text{H-Ni-2}]^-$. Since HER occurred at the second reduction peak experimentally, we further use the relative free energies to compare the formation and reactivity of hydride intermediate from $[\text{Ni-1}]^{2-}$ and $[\text{Ni-2}]^{2-}$, as shown in Fig. 6. Protonation of $[\text{Ni-1}]^{2-}$ by TFA is thermodynamically downhill by 7.7 kcal/mol (Fig. 6a) but



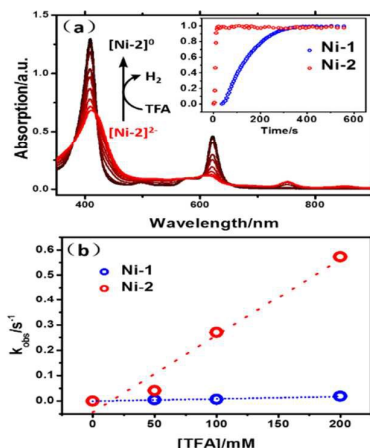


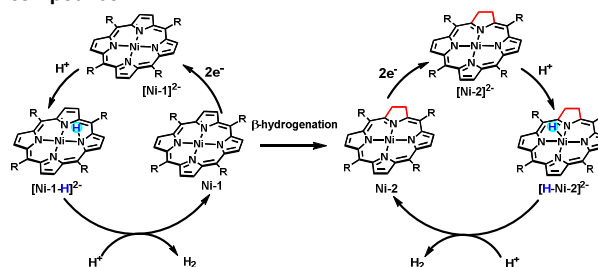
Fig. 7 (a) UV-vis absorption spectra of the process of $[\text{Ni-2}]^{2-}$ reacting with TFA. Inset: Plot of absorption of Soret band vs. time for the reaction of $[\text{Ni-1}]^{2-}$ (blue line) and $[\text{Ni-2}]^{2-}$ (red line) with 100 equiv. TFA at 10 °C. (b) Plot of k_{obs} vs. concentration of TFA for the reaction of $[\text{Ni-1}]^{2-}$ (blue line) and $[\text{Ni-2}]^{2-}$ (red line) with TFA.

protonation of $[\text{Ni-1}]^{-}$ is thermodynamically uphill by 32.2 kcal/mol (Fig. S36). Thus, starting from $[\text{Ni-1}]^{2-}$ is thermodynamically preferred, which is consistent to the experimental CVs that the HER occurring at *ca.* -1.80V. The resulted exothermal product $[\text{Ni-1-H}]^{-}$ was formed through a stretching vibration between H and N transition state TS1 with energy barrier by 18.5 kcal/mol. To find the protonation intermediate, four protonation sites have been tested: *meso*-carbon (metallophlorin intermediate), β -carbon, pyrrolic nitrogen and the nickel center (metal hydride), and we choose the most thermodynamically favored pyrrolic nitrogen protonated one as intermediate. In addition, for the pyrrolic nitrogen, we can indeed find a transition state (Fig. S35c). IRC path shows that H-atom goes through a stretching vibration and the porphyrin ring changes from the flat to ruffle. This phenomenon indicates the protonation of $[\text{Ni-1}]^{2-}$ to $[\text{Ni-1-H}]^{-}$, since $[\text{Ni-1}]^{2-}$ is a triplet flat and $[\text{Ni-1-H}]^{-}$ is a bent singlet. Then, $[\text{Ni-1-H}]^{-}$ can react with another TFA to release H_2 exothermically by 22.3 kcal/mol, regenerating the neutral $[\text{Ni-1}]^0$. For Ni-2, protonation of $[\text{Ni-2}]^{-}$ and $[\text{Ni-2}]^{2-}$ are both thermodynamically uphill by 29.5 and 4.8 kcal/mol, respectively, and $[\text{Ni-2}]^{2-}$ is thermodynamically favourable (Fig. S37). To find the protonation intermediate for Ni-2, the four protonation sites also have been tested, and the most thermodynamically favored metal hydride was chosen. We can also find a transition state (Fig. S35d) and IRC path shows the generation of $[\text{H-Ni-2}]^{-}$ is through a transition state TS2 with energy barrier by 15.2 kcal/mol which is 3.3 kcal/mol lower than TS1. The reaction between $[\text{H-Ni-2}]^{-}$ with another proton is also exothermic by 31.9 kcal/mol.

Interestingly, for $[\text{Ni-2}]^{2-}$, the proton of TFA approaches to the electron rich nickel center with the distance of 1.49 Å,

obliquely to the pyrrolic nitrogen in porphyrin ring, and thus indicates a metal hydride like intermediate $[\text{H-Ni-2}]^{-}$ (Fig. 6c).

Scheme 3. Proposed mechanism for HER catalyzed by a nickel compounds.



However, in $[\text{Ni-1}]^{2-}$, the proton bonds to the pyrrolic nitrogen and formed an N-H bond with a distance of 1.02 Å. Further insights into bonding characteristics of proton adducts is gained from analysis of the Mulliken atomic charges of $[\text{Ni-1-H}]^{-}$ (0.397) and $[\text{H-Ni-2}]^{-}$ (-0.016). (Fig. S33) This demonstrated that hydrogen atom of $[\text{Ni-2-H}]^{-}$ is more electronegative to the hydride of $[\text{H-Ni-1}]^{-}$, and might prefer to react with another TFA molecule via a heterolytic pathway.

Spectroelectrochemical TFA titration of $[\text{Ni-1}]^{2-}$ and $[\text{Ni-2}]^{2-}$.

To verify the reactivity of the two intermediates, $[\text{Ni-1}]^{2-}$ and $[\text{Ni-2}]^{2-}$, we carried out redox titration of nickel complexes in acetonitrile solution using $\text{Co}(\text{Cp}^*)_2$ ($E_{\text{ox}} = -1.90 \text{ V vs. Fc}^+/\text{Fc}$) as a chemical reductant. The one-electron oxidation potential of $\text{Co}(\text{Cp}^*)_2$ is lower than the two-electron reduction potential of Ni-1 and Ni-2. Thus, addition of $\text{Co}(\text{Cp}^*)_2$ led to the formation of $[\text{Ni-1}]^{2-}$ or $[\text{Ni-2}]^{2-}$, which is evidenced by the similar UV-vis absorption spectra to that obtained in spectroelectrochemistry (Fig. S29-30). The addition of excess TFA to the solution of $[\text{Ni-1}]^{2-}$ or $[\text{Ni-2}]^{2-}$ resulted in fast conversion to Ni-1 or Ni-2 (Fig. 7a), accompanied with the formation of H_2 bubble. The overall two-step kinetics reaction mechanisms of H_2 production were shown in Scheme 2 (pathway A). The first proton adding step might be very fast and the second step might be the rate-determining step.^{27a, 27b, 27c} As shown in Fig. 7a, $[\text{Ni-2}]^{2-}$ displayed much larger k_{obs} (0.27 s^{-1}) than $[\text{Ni-1}]^{2-}$ ($6.2 \times 10^{-3} \text{ s}^{-1}$) (pseudo-first-order kinetic model), as exemplified in presence of 100 *equiv.* TFA at 10 °C. Secondary reaction kinetics constants k_2s for $[\text{Ni-1}]^{2-}$ and $[\text{Ni-2}]^{2-}$ of 9.17×10^{-2} and $3.03 \text{ M}^{-1} \text{ s}^{-1}$ respectively, were obtained by linearly fitting k_{obs} s vs. TFA concentration (Fig. 7b). Similar enhancement of titration reaction rates to electrocatalytic HER clearly demonstrated the importance of disrupted conjugation on the electronic structures and the reactivity of reduced Ni complexes, which is consistent to DFT calculation results.

Conclusion

Taken together, we demonstrated for the first time, β -hydrogenation of porphyrin is important on enhancing the HER reactivity using nickel porphyrinoids. Experimental and theoretical studies showed that β -hydrogenation significantly affects the electronic structures of two-electron reduced Ni

Chemical Science Accepted Manuscript

Open Access Article. Published on 19 June 2017. Downloaded on 20/06/2017 02:33:56. This article is licensed under a Creative Commons Attribution-NonCommercial 3.0 Unported Licence.



complexes and renders more electron density localized on Ni center in [Ni-2]²⁻ and [Ni-4]²⁻ than [Ni-1]²⁻ and [Ni-3]²⁻. Thus, as shown in Scheme 3., protonation of [Ni-2]²⁻ leads to a typical metal hydride intermediate [H-Ni-2]²⁻, while [Ni-1]²⁻ only affords a ligand centred hydride [Ni-1-H]²⁻. [H-Ni-2]²⁻ prefers to react with another proton via a quick heterolytic pathway as demonstrated by the time course results of reacting with TFA. This work also provides an opportunity to further design of metal molecular catalysts with subtle structural changes of ligands inspired by natural metal cofactors.

Experimental Section

General Procedures. Commercially available solvents were used after being purified by the Mbraun SPS-800 Solvent Purification System. Deuterium solvents were stored with 4 Å molecular sieves. Manipulations of air and moisture sensitive materials were performed in glove box in an atmosphere of argon. CH₃CN and dimethylformamide was distilled and degassed before use. Tetrabutylammonium hexafluorophosphate (ⁿBu₄NPF₆) was recrystallized from absolute ethanol. Other reagents were purchased from commercial suppliers and used without purification. UV/Vis spectra were recorded on an Agilent 8453 UV/Vis spectrometer equipped with a Agilent 89090A thermostat (±0.1 °C). ESI-MS were recorded on Bruker APEX IV Fourier Transform Ion Cyclotron Resonance Mass Spectrometer using electrospray ionization. ¹H, ¹⁹F and ¹³C NMR spectra were recorded on Bruker-400 MHz NMR. All ¹H NMR experiments were reported in δ units, parts per million (ppm), all coupling constants were in Hz and measured relative to the signal for residual chloroform (7.26 ppm) in the deuterated solvent CDCl₃. For ¹⁹F NMR spectra, CF₃COOH was used as an external reference at 0 ppm. Transmission electron microscopy were determined by JEM-2100F(JEOL). DLS measurements were performed by using a Laser Light Scattering Spectrometer (ALV/Laser Vertriebsgesellschaft m.b.H), which can detect particle sizes ranging from 1.0 nm-1.0 μm. SEM and EDX were performed by using Hitachi S-4800 field emission scanning electron microscope at an accelerating voltage of 5 and 15 kV, respectively. Elemental analyses were done on Elementar Vario EL CUBE (Germany). Cyclic voltammetry experiments were recorded on Shanghai Chenhua CHI660C electrochemical workstation work, glassy carbon electrode was selected as working electrode, auxiliary electrode was platinum wire electrode and Ag/AgCl was reference electrode. All samples were recorded in acetonitrile with 0.1M tBu₄NPF₆ as electrolyte, the scan rate was 0.1 V s⁻¹ and E_{1/2} were calculated based on peak position for the internal standard FeCp₂ (E_{1/2} = 0.45 V vs. SCE).

Synthesis of free base porphyrinoids 1-4. *Meso*-tetrakis(pentafluorophenyl)porphyrin (1), *meso*-tetrakis(pentafluorophenyl)chlorin (2), *meso*-tetrakis(pentafluorophenyl)porpholactone (3) and *adjacent*-

hydroporpholactone (4) were synthesized according to the literature.^{16c, 17}

Synthesis of Ni-1 to Ni-4:

Typical procedure: Porphyrin free base ligand (0.1 mmol) was refluxed with 30 equiv. of Ni(OAc)₂ (1 mmol, 180 mg) in acetonitrile under nitrogen for 6 hours. The solvent was removed by adding 100 equivalents of water and the residue was purified through silica column.

Ni-1: Isolated yields were over 90%. Eluent: ethyl acetate: petroleum ether, 1:5. ¹H NMR (400 MHz, CDCl₃) δ 8.81 (s, 8H). ¹⁹F NMR (377 MHz, CDCl₃) δ -136.47 (dd, J = 23.2, 7.7 Hz, 8F), -150.17 (m, 4H), -161.32 (dt, J = 22.5, 7.4 Hz, 8F). ¹³C NMR (101 MHz, CDCl₃) δ 142.98 (s), 132.52 (s), 103.09 (s). ESI-MS m/z: Calcd. for C₄₄H₈F₂₀N₄Ni 1029.97831, found 1029.97854. Anal. Calcd for C₄₄H₈F₂₀N₄Ni: C, 51.25; H, 0.78; N, 5.43, found C, 51.29; H, 0.92; N, 5.38.

Ni-2. Isolated yields were 75%. Eluent: ethyl acetate: petroleum ether, 1:10. ¹H NMR (400 MHz, CDCl₃) δ = 8.29 (d, J = 4.9 Hz, 2H), 8.14 (s, 2H), 7.95 (d, J = 5.0 Hz, 2H), 3.93 (s, 4H). ¹⁹F NMR (377 MHz, CDCl₃) δ = -136.94 (dd, J=23.2, 7.7Hz, 4F), -137.89 (dd, J=23.8, 8.3Hz, 4F), -151.88 (t, J=20.9Hz, 2F), -152.10 (t, J=20.9Hz, 2F), -160.66 (dt, J=23.3, 8.0Hz, 4F), -161.57 (dt, J=22.6, 7.4Hz, 4F). ¹³C NMR (101 MHz, CDCl₃) δ 169.03 (s), 152.66 (s), 140.39 (s), 135.31 (s), 132.27 (s), 128.22 (s), 123.62 (s), 106.31 (s), 96.83 (s), 35.31 (s, -CH₂-). ESI-MS m/z: Calcd. For C₄₄H₁₀F₂₀N₄Ni 1031.99396, found 1031.98981. Anal. Calcd for C₄₄H₁₀F₂₀N₄Ni: C, 51.15; H, 0.98; N, 5.42, found C, 51.16; H, 1.14; N, 5.31.

Ni-3. Isolated yields were over 90%. Eluent: ethyl acetate: petroleum ether, 1:5. ¹H NMR (400 MHz, CDCl₃) δ 8.67 (d, J = 5.1 Hz, 1H), 8.65 – 8.61 (m, 2H), 8.58 (d, J = 5.1 Hz, 1H), 8.55 (d, J = 4.9 Hz, 2H). ¹⁹F NMR (377 MHz, CDCl₃) δ -136.69 – -136.96 (m), -138.17 – -138.39 (m), -150.28 – -150.62 (m), -151.20 (q, J = 20.9 Hz), -160.27 – -160.87 (m), -161.37 (qd, J = 22.1, 6.8 Hz). ¹³C NMR (101 MHz, CDCl₃) δ 163.03 (s), 149.75 (s), 144.95 (s), 134.45 (s), 132.47 (d), 131.78 (s), 131.17 (s), 130.34 (s), 120.59 (s). ESI-MS m/z: Calcd. For C₄₃H₆F₂₀N₄NiO₂ 1048.95556, found 1048.95959. Anal. Calcd for C₄₃H₆F₂₀N₄NiO₂: C, 49.23; H, 0.58; N, 5.34, found C, 48.66; H, 0.67; N, 5.26.

Ni-4. Isolated yields were over 90%. Eluent: ethyl acetate: petroleum ether, 1:5. ¹H NMR (400 MHz, CDCl₃) δ 7.97 (d, J = 4.8 Hz, 1H), 7.77 (dd, J = 20.5, 4.5 Hz, 2H), 7.54 (d, J = 4.7 Hz, 1H), 3.76 (d, J = 8.4 Hz, 2H), 3.66 (d, J = 8.4 Hz, 2H). ¹⁹F NMR (377 MHz, CDCl₃) δ -137.63 (d, J = 23.9 Hz), -137.89 (d, J = 15.5 Hz), -138.76 (d, J = 15.8 Hz), -151.16 (d, J = 34.0 Hz), -151.50 (s), -151.79 (s), -160.07 (d, J = 6.2 Hz), -160.31 (d, J = 5.9 Hz), -160.68 (d, J = 6.1 Hz), -161.42 (d, J = 5.9 Hz). ¹³C NMR (101 MHz, CDCl₃) δ 165.72 (s, -C=O), 162.06 (s), 156.20 (s), 151.18 (s), 149.93 (s), 141.77 (s), 139.34 (s), 138.75 (s), 133.28 (s), 127.83 (s), 126.19 (s), 115.90 (s), 96.88 (s), 82.19 (s), 34.40 (s, -CH₂-), 32.29 (s, -CH₂-). Calcd. For C₄₃H₈F₂₀N₄NiO₂ [M+H]⁺ 1050.97586, found 1050.97686. Anal. Calcd for C₄₃H₈F₂₀N₄NiO₂: C, 49.13; H, 0.77; N, 5.33, found C, 48.96; H, 0.93; N, 5.20.



Cyclic Voltammetry. Cyclic voltammetry was performed with a CHI 660C instrument. A glassy carbon (3 mm diameter) was used as working electrode, a platinum filament as counter electrode, Ag/AgCl as reference electrode. Solvents were purified by a Mbraun SPS-800 Solvent Purification System. All samples were recorded in dichloromethane with 0.1M ${}^n\text{Bu}_4\text{NPF}_6$ as electrolyte. Unless otherwise noted, all potentials in this study were adjusted ferrocenium/ferrocene ($\text{Fc}^{+/0}$) couple as internal standard.

Spectroelectrochemistry Studies. Spectroelectrochemical measurements were carried out in a quartz cell with an optical path length of 1 cm. A platinum net, a platinum filament and Ag/AgCl were used as working electrode, counter electrode, and reference electrode, respectively. The sample solutions were deaerated with acetonitrile-saturated argon. The spectra were recorded on an Agilent 8453 UV-vis spectrophotometer during electrolysis on a CHI 660C instrument.

Controlled-voltage coulometry experiment. Bulk electrolysis was performed with a CHI 660C instrument with a glassy carbon (1 cm \times 1 cm) as working electrode. The reference electrode was an aqueous Ag/AgCl electrode, and the counter electrode was a platinum wire and 0.1 M ${}^n\text{Bu}_4\text{NPF}_6$ in CH_3CN solution. The volume of the electrolysis solution was 20 mL. The reference electrode was directly immersed in the solution to minimize Ohmic drop. The gas phase in the head space was analyzed by GC with Ar as carrying gas. Hydrogen calibration curve was obtained by filling pure hydrogen gas to a tube with a graduated gastight syringe.

Chemistry titration. Acetonitrile solutions of Ni-1 or Ni-2 (1.6×10^{-5} M) and $\text{Co}(\text{Cp}^*)_2$ (9.3×10^{-4} M) were prepared in the glove box and stored in airtight cuvettes and vial respectively. The solution of Ni-1 or Ni-2 and 25 μL $\text{Co}(\text{Cp}^*)_2$ (1 equivalent) was mixed and the UV-vis spectra were recorded immediately after the mixing.

Computational details. All geometry optimizations calculations were performed using the density functional theory (DFT) functional B3LYP/6-31G+(d) as basis set and LAN2DZ as pseudopotential as implemented in the Gaussian 09 software. Solvent effect was considered in all geometry optimizations and property calculations using the conductor-like polarizable continuum model (CPCM). The energies were corrected by single point calculations using B3LYP/6-31+G(d,p) as basis set. For the absolute solvation free energy of the proton in acetonitrile, a value of $-260.2 \text{ kcal mol}^{-1}$ was used.²⁸ The frequency calculations at the same level were carried out to confirm each stationary point to be either a minimum or transition state. Intrinsic reaction coordinate (IRC) paths were calculated to connect each TS to corresponding reactant and product.

Acknowledgements

We acknowledge financial support from the National Key Basic Research Support Foundation of China (Grant 2015CB856301) and the National Scientific Foundation of China (Grants

21571007, 21271013, 21321001). X. R. He is gratefully thanked for help with the ESI-MS. Z.-C. Huang and H. Zhu are gratefully thanked for help with the DFT calculation parts. T. Huang is gratefully thanked for help with DLS. T.-T. Zuo is gratefully thanked for help with TEM. Y.-Y. Yuan is gratefully thanked for help with SEM and EDX.

Notes and references

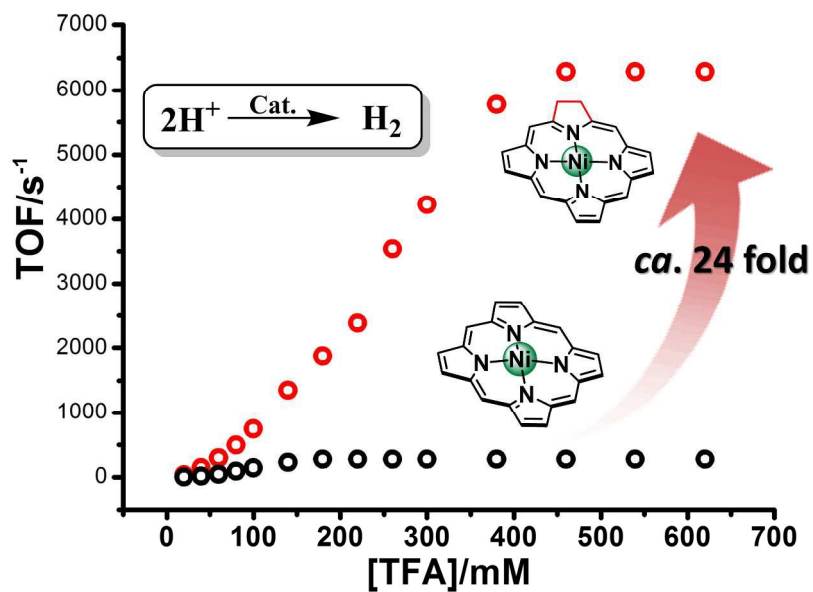
- (a) K. M. Kadish, K. M. Smith and R. Guilard, *Handbook of porphyrin science : with applications to chemistry, physics, materials science, engineering, biology and medicine*, World Scientific, 2014; (b) H.-B. Kraatz and N. Metzler-Nolte, *Concepts and models in bioinorganic chemistry*, Wiley-VCH New York, 2006; (c) Y. M. Sung, J. Oh, W. Y. Cha, W. Kim, J. M. Lim, M. C. Yoon and D. Kim, *Chem. Rev.*, 2016, **117**, 2257; (d) R. D. Teo, J. Y. Hwang, J. Termini, Z. Gross and H. B. Gray, *Chem. Rev.*, 2016, **114**, 2177; (e) W. Zhang, W. Lai and R. Cao, *Chem. Rev.*, 2016, **117**, 3717.
- (a) L.-L. Li and E. W.-G. Diao, *Chem. Soc. Rev.*, 2013, **42**, 291-304; (b) M. R. Wasielewski, *Acc. Chem. Res.*, 2009, **42**, 1910-1921.
- (a) M. Ethirajan, Y. Chen, P. Joshi and R. K. Pandey, *Chem. Soc. Rev.*, 2011, **40**, 340-362; (b) A. P. Castano, P. Mroz and M. R. Hamblin, *Nat. Rev. Cancer*, 2006, **6**, 535-545.
- (a) C. M. Drain, A. Varotto and I. Radivojevic, *Chem. Rev.*, 2009, **109**, 1630; (b) R. Paolesse, S. Nardis, D. Monti, M. Stefanelli and C. Di Natale, *Chem. Rev.*, 2017, **117**, 2517-2583; (c) Y. Ding, W. H. Zhu and Y. Xie, *Chem. Rev.*, 2016, **117**, 2203.
- (a) M. Kruger, A. Meyerdierks, F. O. Glockner, R. Amann, F. Widdel, M. Kube, R. Reinhardt, R. Kahnt, R. Bocher, R. K. Thauer and S. Shima, *Nature*, 2003, **426**, 878-881; (b) T. J. Lawton and A. C. Rosenzweig, *J. Am. Chem. Soc.*, 2016, **138**, 9327-9340.
- (a) W. L. Ellefson, W. B. Whitman and R. S. Wolfe, *Proc. Natl. Acad. Sci. USA*, 1982, **79**, 3707-3710; (b) S. J. Moore, S. T. Sowa, C. Schuchardt, E. Deery, A. D. Lawrence, J. V. Ramos, S. Billig, C. Birkemeyer, P. T. Chivers, M. J. Howard, S. E. Rigby, G. Layer and M. J. Warren, *Nature*, 2017, **543**, 78-82.
- (a) K. C. Bible, M. Buytendorp, P. D. Zierath and K. L. Rinehart, *Proc. Natl. Acad. Sci. USA*, 1988, **85**, 4582-4586; (b) L. A. Andersson, A. Huff and K. M. Smith, *Biophys. J.*, 1990, **57**, A232-A232.
- (a) K. Kadish, M. Franzen, B. Han, C. Araullo-McAdams and D. Sazou, *J. Am. Chem. Soc.*, 1991, **113**; (b) J. Telsler, Y.-C. Fann, M. W. Renner, J. Fajer, S. Wang, H. Zhang, R. A. Scott and B. M. Hoffman, *J. Am. Chem. Soc.*, 1997, **119**, 733-743; (c) A. Atifi and M. D. Ryan, *Anal. Chem.*, 2015, **87**, 12245-12253; (d) F. V. Lovecchio, E. S. Gore and D. H. Busch, *J. Am. Chem. Soc.*, 1974, **96**, 3109-3118.
- (a) H. B. Gray, *Nat. Chem.*, 2009, **1**, 7-7; (b) D. Gust, T. A. Moore and A. L. Moore, *Acc. Chem. Res.*, 2009, **42**, 1890-1898; (c) C. G. Moralesguio, L. A. Stern and X. Hu, *Chem. Soc. Rev.*, 2014, **43**, 6555-6569; (d) J. X. Jian, C. Ye, X. Z. Wang, M. Wen, Z. J. Li, X. B. Li, B. Chen, C. H. Tung and L. Z. Wu, *Energy Environ. Sci.*, 2016, **9**, 2083-2089.
- (a) M. Wang, L. Chen and L. Sun, *Energy Environ. Sci.*, 2012, **5**, 6763-6778; (b) P. Du and R. Eisenberg, *Energy Environ. Sci.*, 2012, **5**, 6012-6021; (c) V. S. Thoi, Y. Sun, J. R. Long and C. J. Chang, *Chem. Soc. Rev.*, 2013, **42**, 2388-2400; (d) J. R. Mckone, S. C. Marinescu, B. S. Brunshwig, J. R. Winkler and H. B. Gray, *Chem. Sci.*, 2014, **5**, 865-878; (e) J. Ran, J. Zhang, J. Yu, M. Jaroniec and S. Z. Qiao, *Chem. Soc. Rev.*, 2014, **43**, 7787-7812; (f) B. Mondal, K.



- Sengupta, A. Rana, A. Mahammed, M. Botoshansky, S. G. Dey, Z. Gross and A. Dey, *Inorg. Chem.*, 2013, **52**, 3381-3387.
- 11 (a) W. Lubitz, H. Ogata, O. Ruediger and E. Reijerse, *Chem. Rev.*, 2014, **114**, 4081-4148; (b) J. P. Layfield and S. Hammes-Schiffer, *Chem. Rev.*, 2014, **114**, 3466-3494.
- 12 (a) H. Lu and X. P. Zhang, *Chem. Soc. Rev.*, 2011, **40**, 1899-1909; (b) C.-M. Che, V. K.-Y. Lo, C.-Y. Zhou and J.-S. Huang, *Chem. Soc. Rev.*, 2011, **40**, 1950-1975; (c) C. Kupitz, R. Fromme, I. Grotjohann and P. Fromme, in *Handbook of Porphyrin Science with Applications to Chemistry, Physics, Materials Science, Engineering, Biology and Medicine*, eds. G. C. Ferreira, K. M. Kadish, K. M. Smith and R. Guilard, World Scientific, Singapore, 2014, vol. 28, pp. 1-40; (d) M. O. Senge, S. A. MacGowan and J. M. O'Brien, *Chem. Commun.*, 2015, **51**, 17031-17063; (e) W. Zhang, W. Lai and R. Cao, *Chem. Rev.*, 2017, **117**, 3717-3797.
- 13 Y. Han, H. Fang, H. Jing, H. Sun, H. Lei, W. Lai and R. Cao, *Angew. Chem. Int. Ed. Engl.*, 2016, **55**, 5457-5462.
- 14 D. K. Bediako, B. H. Solis, D. K. Dogutan, M. M. Roubelakis, A. G. Maher, C. H. Lee, M. B. Chambers, S. Hammes-Schiffer and D. G. Nocera, *Proc. Natl. Acad. Sci. USA*, 2014, **111**, 15001-15006.
- 15 B. H. Solis, A. G. Maher, D. K. Dogutan, D. G. Nocera and S. Hammes-Schiffer, *Proc. Natl. Acad. Sci. USA*, 2016, **113**, 485-492.
- 16 (a) X.-S. Ke, H. Zhao, X. Zou, Y. Ning, X. Cheng, H. Su and J.-L. Zhang, *J. Am. Chem. Soc.*, 2015, **137**, 10745; (b) X.-S. Ke, Y. Chang, J.-Z. Chen, J. Tian, J. Mack, X. Cheng, Z. Shen and J.-L. Zhang, *J. Am. Chem. Soc.*, 2014, **136**, 9598-9607; (c) Y. Yu, T. Furuyama, J. Tang, Z.-Y. Wu, J.-Z. Chen, N. Kobayashi and J.-L. Zhang, *Inorg. Chem. Front.*, 2015, **2**, 671-677; (d) Y. Ning, X. S. Ke, J. Y. Hu, Y. W. Liu, F. Ma, H. L. Sun and J. L. Zhang, *Inorg. Chem.*, 2017, **56**, 1897-1905.
- 17 Y. Yu, H. Lv, X. Ke, B. Yang and J.-L. Zhang, *Adv. Synth. Catal.*, 2012, **354**, 3509-3516.
- 18 (a) C. Brückner, J. R. McCarthy, H. W. Daniell, Z. D. Pendon, R. P. Ilagan, T. M. Francis, L. Ren, R. R. Birge and H. A. Frank, *Chem. Phys.*, 2003, **294**, 285-303; (b) Y. Yu, B. Czepukojc, C. Jacob, Y. Jiang, M. Zeller, C. Brückner and J.-L. Zhang, *Org. Biomol. Chem.*, 2013, **11**, 4613-4621.
- 19 D. Lexa, M. Momenteau, J. Mispelter and J. M. Saveant, *J. Inorg. Biochem.*, 1989, **28**, 225-225.
- 20 C. J. Campbell, J. F. Rusling and C. Bruckner, *J. Am. Chem. Soc.*, 2000, **122**, 6679-6685.
- 21 (a) A. M. Stolzenberg and M. T. Stershic, *J. Am. Chem. Soc.*, 1988, **110**, 6391-6402; (b) A. M. Stolzenberg and M. T. Stershic, *J. Am. Chem. Soc.*, 1988, **110**, 5397-5403.
- 22 M. W. Renner, L. R. Furenlid, K. M. Barkigia, A. Forman, H. K. Shim, D. J. Simpson, K. M. Smith and J. Fajer, *J. Am. Chem. Soc.*, 1991, **113**, 6891-6898.
- 23 (a) K. M. Kadish, M. M. Franzen, B. C. Han, C. Araullomcadams and D. Sazou, *J. Am. Chem. Soc.*, 1991, **113**, 512-517; (b) M. W. Renner, L. R. Furenlid, K. M. Barkigia, A. Forman, H. K. Shim, D. J. Simpson, K. M. Smith and J. Fajer, *J. Am. Chem. Soc.*, 1991, **113**, 6891-6898.
- 24 (a) C. Costentin, G. Passard and J. M. Savéant, *J. Am. Chem. Soc.*, 2015, **137**, 5461-5467; (b) E. S. Rountree, B. D. McCarthy, T. T. Eisenhart and J. L. Dempsey, *Inorg. Chem.*, 2014, **53**, 9983-10002.
- 25 V. Artero and M. Fontecave, *Coord. Chem. Rev.*, 2005, **249**, 1518-1535.
- 26 I. Bhugun, D. Lexa and J.-M. Savéant, *J. Am. Chem. Soc.*, 1996, **118**, 3982-3983.
- 27 (a) J. Kleperis, G. Wojcik, A. Czerwinski, J. Skowronski, M. Kopczyk and M. Beltowska-Brzezinska, *J. Solid State Electrochem.*, 2001, **5**, 229-249; (b) S. Mandal, S. Shikano, Y. Yamada, Y. M. Lee, W. Nam, A. Llobet and S. Fukuzumi, *J. Am. Chem. Soc.*, 2013, **135**, 15294-15297; (c) N. A. Eberhardt and H. Guan, *Chem. Rev.*, 2016, **116**, 8373-8426.
- 28 Candee C. Chambers, G. D. Hawkins, a. Christopher J. Cramer and D. G. Truhlar, *J. Phys. Chem.*, 1996, **100**, 100-16385.



β -hydrogenation of porphyrin remarkably enhances (ca. 24 folds) electrocatalytic HER reactivity of Ni(II) complexes.



517x387mm (150 x 150 DPI)

